POLISH MARITIME RESEARCH 2 (130) 2026 Vol. 33; pp. 4-17
10.2478/pomr-2026-0016

Numerical Investigation of Icebreaking Resistance of Ships Navigating in Narrow Ice Channels

Junhao Zhao [1]
Bin Mei [1,*]
Weifeng Li [1]
[1] School of Navigation, Dalian Maritime University, Dalian, China

* Corresponding author: *meibindmu@163.com (Bin Mei)*

ABSTRACT

In ice-covered waters, ships may pass through narrow ice channels, where the interactions with the intact ice along the channel boundaries differ from those under level ice conditions. To investigate this problem, numerical simulations of a steel plate impacting on conical sea ice were first conducted to verify a constitutive model developed for ice. Subsequently, based on an explicit dynamic formulation, a coupled ship–ice–water interaction model was developed using an arbitrary Lagrangian–Eulerian algorithm for the fluid–structure interaction. This numerical approach was validated through comparison with the results of ice tank model tests in terms of ice failure patterns and icebreaking resistance, which confirmed the applicability of the proposed model. On this basis, a series of simulations was carried out to examine the icebreaking behaviour of a ship in a narrow channel with varying widths, ship speeds and ice thicknesses. The results showed that the icebreaking resistance in an extremely narrow channel is lower than under level ice conditions, and that the occurrence of lateral cracks is associated with a reduction in resistance. As the channel width was increased, the variation in the resistance became less pronounced. In addition, icebreaking resistance increased with ship speed and ice thickness, and this trend became more evident under confined channel conditions. The findings of this study contribute to the evaluation of ship performance in narrow ice channels and provide reference information for engineering applications in ice-covered waters.

Keywords: Narrow ice channels; ice resistance; ship-ice-water interaction; numerical simulation

INTRODUCTION

Following the accelerated development of polar shipping routes, an increasing number of ships are now navigating in ice-covered waters. During this process, interactions between the ship's hull and sea ice generate significant ice resistance, which not only directly affects the ship's speed and propulsion efficiency but is also a key factor in the structural design and navigational safety assessment of polar ships. Hence, accurate prediction of the icebreaking resistance of ships has become an important research topic in the fields of polar ship and offshore engineering.

During icebreaker escort operations, escorted ships are required to navigate within channels of limited width. Under such conditions, the hull may come into contact with the intact ice along the channel boundaries, which can induce a phenomenon called "secondary icebreaking". When the icebreaking capability of a ship is insufficient for navigation in thick ice, auxiliary operations such as the two-icebreaker assistance mode, oblique navigation mode [1], or bidirectional icebreaking mode [2] are usually required, but these operational strategies significantly increase the complexity of icebreaking operations. Consequently, accurate predictions of ice resistance

for ships navigating in narrow ice channels is of great importance in terms of the optimisation of route planning and deployment of icebreakers, as well as for ensuring the economic feasibility of Arctic navigation.

The main research approaches to the prediction of ship icebreaking resistance can be classified into three types: experimental methods, empirical formula methods, and numerical simulation methods [3]. Experimental methods allow the ice resistance acting on a ship during navigation in ice-covered waters to be measured directly and accurately, and complex physical phenomena such as sea ice fracture and failure can be observed in detail. For example, a systematic summary of full-scale trials conducted on the icebreaker *Tor Viking II* was presented by Riska et al. [4], and model-scale towing tests of an icebreaker were carried out by Zhou et al. [5] in the ice tank at Aalto University, in which the hull ice loads and the ice failure processes were systematically measured and analysed. However, experimental methods are generally associated with long testing periods and high costs, meaning that they lack widespread applicability. Methods based on empirical formulae are widely used for the estimation of ice resistance due to their simplicity and high computational efficiency; commonly used empirical approaches include those proposed by Lindqvist [6], Keinonen et al. [7], Riska et al. [8], and Spencer et al. [9]. These methods are established on the basis of simplified assumptions, and the empirical relationships between ice resistance, hull form, and ice conditions are derived from full-scale measurements and model test data from ice tanks. Consequently, the nonlinear characteristics of complex ship–ice interactions and ice failure processes cannot be adequately captured by these methods.

In view of the limitations of experimental methods in terms of cost and testing duration, as well as the insufficient capability of empirical formulae in describing the complex interactions between the ship and the ice, numerical simulation methods for the study of ship icebreaking resistance have gradually become widespread. Computational simulations are capable of reproducing icebreaking processes under a wide range of operating conditions, and current approaches mainly include the discrete element method (DEM) and the finite element method (FEM). In DEM, sea ice is represented as an assembly of interacting discrete elements, and the fracture of ice and the evolution of broken ice can be described through different bonding and failure models, which offers certain advantages in the simulation of broken ice formation and motion behaviours. Zou et al. [10] investigated the icebreaking process in narrow ice channels using a CFD-DEM coupled method, and analysed the influence of broken ice accumulation on ice loads.

FEM is based on the assumption of a continuous medium, and the deformation and failure of ice are described by introducing material constitutive models together with damage or fracture criteria. This method has been widely applied to the investigation of ship icebreaking resistance and ship–ice interaction problems; for example, in a study conducted by Ren et al. [11], a finite element numerical simulation method based on an arbitrary Lagrangian-Eulerian (ALE) algorithm was adopted, and the influence of different bow shapes on the continuous icebreaking performance of an icebreaker was systematically analysed. In research conducted by Bian et al. [12], FEM was employed to establish numerical simulation models using LS-DYNA software, and the structural safety of an icebreaker under conditions of extremely thick ice was evaluated. Multi-method coupling strategies based on FEM have been adopted in some studies to model large deformations and the motion of broken ice that may occur during the icebreaking process. Diao et al. [13] employed an FEM-SPH-SALE coupled model to overcome the limitations of a mesh for the simulation of large deformations, and explored the dynamic response characteristics during the icebreaking process. In a study carried out by Xu et al. [14], a finite element-smoothed particle hydrodynamics (FEM-SPH) coupled algorithm was adopted to simulate the ship–ice collision processes of polar ships in level ice conditions. Liu et al. [15] constructed a hybrid-parameter sea ice model using the cohesive zone method, and analysed the ice resistance and failure modes during ship–ice collision processes through finite element simulations to verify the applicability of the proposed model. In problems involving ship icebreaking under narrow channel conditions, the constraint effect imposed by the channel boundaries is significant, and the overall deformation capability of ice is limited. Under such conditions, the ALE fluid–structure interaction algorithm is capable of providing an appropriate description of ice failure characteristics. Meanwhile, the constitutive model of ice also plays an important role in determining the simulation results.

In numerical simulation methods, the selection of a constitutive model for the ice has a significant influence on the simulation results. A variety of ice material models have been proposed by researchers for different ice conditions, and corresponding numerical studies have been conducted. Gagnon [16] employed LS-DYNA finite element software to establish a numerical model with a Poisson's ratio of zero, which was capable of simulating ice fragmentation; this model was successfully applied to the numerical simulation of collisions between the icebreaker *CCGS Terry Fox* and floating ice. Kim et al. [17] developed a constitutive model for the compressive failure of sea ice based on the Drucker–Prager criterion and continuum damage mechanics, and verified the compressive failure process through numerical simulations. The proposed model was then applied to analysis of the ship–ice interaction. Xu et al. [18] established an constitutive model for ice material that accounted for strain rate and temperature effects, and confirmed its capability to describe the mechanical behaviour of ice through numerical simulations.

In a study of ship resistance in narrow ice channels, Sazonov et al. [19] proposed a simplified method for evaluating ship ice resistance during navigation in channels opened by icebreakers, based on improvements to empirical resistance methods for level ice and broken ice, which was developed at the Krylov ice tank. Li et al. [[20]] analysed the influence of the channel width on the ship's resistance and attainable speed through model tests conducted in the ice tank at Aalto University, in combination with ASOIS numerical simulations. Dong et al. [21] carried out numerical simulations of ship–ice collision processes under narrow ice channel conditions using MSC.Dytran, and analysed the structural response characteristics. Numerical investigations based on CFD-DEM coupling have also been carried out to

examine channel restriction effects and broken ice accumulation in pack ice channels [10].

The number of existing studies of ship resistance under narrow ice channel conditions remains relatively limited. In this environment, the ship's ice resistance mainly originates from the contact and failure processes between the hull and the continuous ice sheets along both sides of the channel, with a response that exhibits pronounced nonlinear and transient characteristics. The explicit dynamic method is capable of effectively handling complex contact and transient response processes, and is therefore suitable for the simulation of such ship–ice–water interaction problems.

Building on the research described above in the area of numerical simulation methods and ice material constitutive models, the present study focuses on the problem of ship icebreaking resistance under narrow ice channel conditions in ice-covered waters. The remainder of this paper is structured as follows. Section 2 introduces the numerical simulation methodology, and demonstrates the rationality of the ice material model. Section 3 validates the numerical model for icebreaking in level ice conditions. Section 4 describes numerical simulations for ship navigation scenarios in narrow ice channels in ice-covered waters. Section 5 analyses the factors influencing a ship's icebreaking resistance under narrow ice channel conditions.

The main innovative aspects of the present study are as follows:

(1) For icebreaking scenarios involving narrow ice channels, an explicit dynamic method was adopted in this study, and multiple constitutive models were employed to simulate ice materials. The applicability of the constitutive models was verified, and a numerical model for ship–ice–water interaction was established using an ALE algorithm for the fluid–structure interaction.
(2) Time histories of ship icebreaking resistance under narrow ice channel conditions were obtained through numerical simulations. The icebreaking resistance caused by extremely small ice cracks was also derived using an extrapolation algorithm, thereby demonstrating the influence of ice cracks on ice resistance.
(3) By comparing the differences in ice resistance between narrow ice channel conditions and level ice conditions, the characteristics of the variation in icebreaking resistance in narrow ice channels were identified.

NUMERICAL METHOD FOR ICEBREAKING IN NARROW ICE CHANNELS

CLASSIFICATION OF NARROW ICE CHANNELS IN ICE-COVERED WATERS

In icebreaker-assisted escort operations, the ice resistance acting on a ship navigating in a narrow channel generally consists of two components: (i) displacement of the residual broken ice within the channel, and (ii) breaking and subsequent displacement of the intact ice sheets along the channel edges. In the channels created by modern icebreakers, the amount of residual broken ice largely depends on the clearing capability of the leading vessel. As reported by Huang et al. [22], certain icebreaker designs enable broken ice to be pushed downward and laterally beneath adjacent intact ice sheets, thereby forming relatively clear escort channels. These channels differ fundamentally from brash ice channels, which are typically characterised by a high ice concentration, increased ice thickness, and significant accumulation of rubble. In some cases, the residual ice concentration may be sufficiently low to approximate open-water conditions.

Consistent with these observations, and following previous model-scale and numerical studies conducted under narrow open-water channel conditions, the present study focuses on the interaction between the ship's hull and the intact ice sheets along the channel boundaries, which is assumed to constitute the dominant component of the resistance. The contribution of broken ice within the channel is therefore neglected; this assumption corresponds to an idealised icebreaker-cleared channel condition, and does not represent operations in brash ice channels with substantial accumulation of rubble. For channel conditions involving a significant presence of broken ice, approaches that explicitly take into account the motion of discrete ice pieces, such as CFD-DEM methods, may provide a more comprehensive description of the resistance components.

In the present study [20], the non-dimensional channel width γ is defined as the ratio between the physical channel width w and the moulded ship breadth B, i.e.

$$\gamma = \min\left(\frac{w}{B}, 1\right) \tag{1}$$

where w represents the clear distance between the two intact ice boundaries, and B denotes the moulded breadth of the ship at the design waterline.

According to this definition, $\gamma = 0$ corresponds to the condition of intact, level ice with no pre-existing channel, whereas $\gamma = 1$ represents a channel with a width equal to the ship's breadth. For values in the range $0 < \gamma < 1$, the configuration is classified as a narrow ice channel, where geometric confinement effects are present. For the purpose of describing the relative magnitude of the channel width with respect to the ship's breadth, five levels are defined for the channel width, as shown in Fig. 1: a channel with γ approximately equal to 1/4 is referred to as a slightly open channel, whereas a channel with a value of γ of approximately 1/2 is referred to as a half-open channel, a value for γ of approximately 3/4 represents a largely half-open channel, and a value of 7/8 represents a nearly fully open channel. A channel with γ equal to one is referred to as a fully open channel.

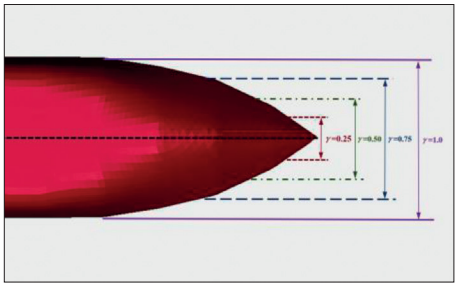

Fig. 1. Classification of narrow ice channels

Note: The channel width w is defined as the clear distance between the intact ice boundaries.

FINITE ELEMENT EXPLICIT DYNAMICS AND THE FLUID–STRUCTURE INTERACTION ALGORITHM

Formulation of ship–ice collision equations

The finite element explicit solution method is an important approach for addressing nonlinear dynamic contact and collision problems. In this method, the basic idea is to discretise the continuous solution domain into a numerical model composed of element nodes, in which a finite number of variables are employed to approximate the infinite degrees of freedom of the actual system, thereby obtaining numerical solutions. This method is characterised not only by relatively high computational accuracy, but also by strong adaptability to different element shapes. As a result, complex geometrical features of the hull surface and corresponding boundary conditions can be accurately represented.

For strongly nonlinear dynamic problems such as collisions between polar ships and ice sheets, an explicit solution strategy is considered to be appropriate. The corresponding process can be described by the following equation of motion [23]:

$$M\ddot{x}_n + C\dot{x}_n + Kx_n = F_n^{ext} \tag{2}$$

where M denotes the mass matrix, C denotes the damping matrix, and K denotes the stiffness matrix. The vectors $\ddot{x}_n$, $\dot{x}_n$ and x_n represent the nodal acceleration vectors at time t_n, respectively, and t F_n^{ext} denotes the external load vector at time t_n.

Let

$$F_n^{int} = C\dot{x}_n + Kx_n \tag{3}$$

Then, from Eq. (2), the following expression can be obtained:

$$M\ddot{x}_n = F_n^{ext} - F_n^{int} \tag{4}$$

Let

$$F_n^{residual} = F_n^{ext} - F_n^{int} \tag{5}$$

where $F_n^{residual}$ denotes the residual force vector at time t.

$$M\ddot{x}_n = F_n^{residual} \tag{6}$$

Accordingly, the nodal acceleration can be obtained as:

$$\ddot{x}_n = M^{-1} F_n^{residual} \tag{7}$$

By applying the lumped mass assumption, the global mass matrix M becomes a diagonal matrix. When computing the nodal accelerations, this approach avoids the need to perform complex operations on the stiffness matrix K, and only requires inversion of the simple diagonal mass matrix M, which significantly improves the computational efficiency.

Based on the assumption that the acceleration remains constant within a single time step, and by applying an explicit central difference scheme in the time domain, the form of the solution to Eq. (7) can be written as:

$$\begin{cases} \dot{x}(t_{n+\frac{1}{2}}) = \dot{x}(t_{n-\frac{1}{2}}) + \frac{1}{2}(\Delta t_{n-\frac{1}{2}} + \Delta t_{n+\frac{1}{2}})\ddot{x}(t_n) \\ x(t_{n+1}) = x(t_n) + \dot{x}(t_{n+\frac{1}{2}})\Delta t_{n+\frac{1}{2}} \\ t_{n-\frac{1}{2}} = \frac{1}{2}(t_n + t_{n-1}),\ t_{n+\frac{1}{2}} = \frac{1}{2}(t_n + t_{n+1}) \\ \Delta t_{n+\frac{1}{2}} = \frac{1}{2}(\Delta t_n + \Delta t_{n+1}),\ \Delta t_n = (t_n - t_{n-1}),\ t_{n+1} = (t_{n+1} - t_n) \end{cases} \tag{8}$$

where $x(t_{n+1})$ is the displacement vector at time t_{n+1}, $\dot{x}(t_{n+\frac{1}{2}})$ is the velocity vector at time $t_{n+\frac{1}{2}}$, and $\dot{x}(t_{n-\frac{1}{2}})$ is the velocity vector at time $t_{n-\frac{1}{2}}$.

From Eq. (8), it can be seen that the nodal displacement $x(t_{n+1})$ at time t_{n+1} can be obtained from the displacement at time t_n and the velocity at time $t_{n+\frac{1}{2}}$.Through step-by-step recursive calculations based on the recurrence relations given above, the nodal displacements, velocities, and accelerations at each discrete time point can be successively obtained. The procedure set out above constitutes the main solution process of the explicit time integration method. The system of linear equations involved in this method is non-coupled and can therefore be solved directly, which allows for a significant reduction in both the memory storage requirements and computational time for numerical simulations.

Fluid–structure interaction algorithm

The fluid–structure interaction method is applicable to the interaction between large-scale structures and fluid domains, and yields more realistic simulations of the ship–ice collision process. LS-DYNA provides three numerical algorithms, namely the Lagrangian method, the Eulerian method, and the ALE method, as illustrated in Fig. 2. Although the Lagrangian method is suitable for solid structure analysis, large deformations can easily lead to mesh distortion, whereas the Eulerian method is suitable for fluid problems involving large deformations but has difficulty in accurately capturing the motion of the interface. The ALE method combines the advantages of both approaches, as it allows the mesh to move independently, thereby enabling effective tracking of the material boundaries while avoiding mesh distortion. This means that the ALE method is particularly suitable for the analysis of ship–ice–water interaction problems.

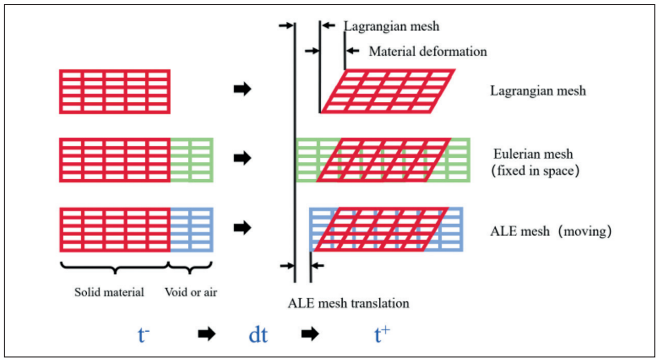

Fig. 2. Simulated motion of a solid material with three different algorithms

In this study, the ALE method was adopted for numerical simulations of the ship–ice collision process. The structure of the ship and the sea ice were modelled using a Lagrangian mesh, so that the structural deformation could be accurately captured, while the water and air were described using an ALE mesh in

order to avoid mesh distortion. The coupling between the two domains was achieved through the keyword *CONSTRAINED_LAGRANGE_IN_SOLID based on the penalty function method, thereby enabling efficient and accurate simulation of the complex ship–ice–water interaction.

ESTABLISHMENT OF THE FINITE ELEMENT MODEL

Finite element model of the hull

The icebreaking oil tanker *MT Uikku* was selected as the research object for this study. This vessel was designed in accordance with the requirements of the Finnish–Swedish Ice Class Rules for the highest ice class, known as IA Super. Zhou et al. [24] previously conducted a series of model-scale ice tank experiments for this vessel. The model of the ship was based on a flat-bottom keel design without a deadrise angle, and the geometric scale ratio of the model was 1:31.6. The principal dimensions of the ship are given in Table 1. Since the publicly available model test data [24] had been converted to full-scale values by Zhou et al. using the dynamic similarity criterion, based on the dynamic similarity criterion, the numerical model in the present study was established directly using full-scale parameters.

Tab. 1. Principal dimensions of the icebreaking oil tanker MT Uikku

Item	Full scale	Model scale
Length [m]	150	4.75
Moulded breadth [m]	21	0.67
Tested draft [m]	9.5	0.30
Bow waterline angle	21	21
Bow stem angle [deg]	30	30
Block coefficient	0.72	0.72

Fig. 3. MT Uikku and the finite element model used in the simulations

In this section, the primary focus is on sea ice crushing, crack propagation, and the numerical magnitude of the ice resistance, whereas the damage to the icebreaking vessel and its deformation during the collision process are not considered. The icebreaking vessel is therefore modelled as a rigid steel body [25]. The material parameters of the ship structure are given in Table 2.

Tab. 2. Material properties of the ship structure

Material property	Full scale
Density [kg·m^{-3}]	7850
Young's modulus	200
Poisson's ratio	0.3

Finite element model of level ice and its validation

In numerical simulations of ship–ice collisions, the selection of an appropriate constitutive model for the ice is a key factor governing the reliability of the results. In the present study, an isotropic elastic–plastic fracture model is adopted to represent sea ice, following the formulation reported in [15]. The corresponding material parameters are summarised in Table 3. The parameters can generally be classified into two categories: the first comprises fundamental physical properties, such as density and elastic moduli, which are directly obtained from experimental measurements available in the literature, while the second includes phenomenological parameters associated with yielding and fracture (e.g. yield stress, cut-off pressure and plastic failure strain). These parameters cannot be uniquely determined from dimensional analysis, and values are therefore selected based on previous numerical studies and established engineering practice. In the present work, the chosen values are consistent with commonly adopted ranges for simulations of ship–ice interaction.

Tab. 3. Material parameters of sea ice

Material property	Full scale
Density [kg·m^{-3}]	910
Shear modulus [Pa]	2.20×10^9
Bulk modulus [Pa]	5.26×10^9
Yield stress [Pa]	2.12×10^6
Cut-off pressure [Pa]	-4×10^6
Plastic failure strain	0.35

A conical ice specimen was defined with a base radius of 5 m and a height of 5 m, with all nodes on the base of the cone fully constrained. The steel plate was modelled as a square plate with a side length of 10 m and a thickness of 2 mm, and a rigid material model was adopted. The initial distance between the steel plate and the front surface of the sea ice was set to 1 mm. The steel plate impacted on the sea ice vertically, with a velocity of 10 m/s, and stopped after reaching a penetration depth of 4 m into the cone. In the numerical simulation, a surface-to-surface contact formulation with an erosion algorithm was employed to model the contact between the steel plate and the conical sea ice. When ice elements fail, LS-DYNA automatically searches for the next contact nodes, thereby ensuring the stability of the contact. The specific keyword settings are listed in Table 4. Fig. 4 shows the finite element model of the steel plate impacting on the conical sea ice.

Tab. 4. Keyword settings

Keyword	Description
*CONTACT_ERODING_SURFACE_TO_SURFACE_ID	Defines the contact interaction between the steel plate and sea ice
*CONTACT_ERODING_SINGLE_SURFACE	Defines the single-surface eroding contact within sea ice
*BOUNDARY_PRESET_MOTION_RIGID	Defines the prescribed initial impact motion of the steel plate
*CONTROL_TIMESTEP	Defines the computational time tep

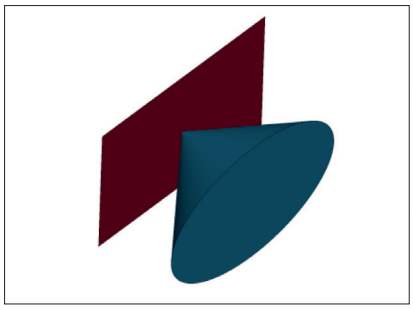

Fig. 4. Finite element model of a steel plate impacting on conical sea ice

During the collision between the steel plate and conical sea ice, most ice elements in the contact zone reach the failure strain owing to the movement of the steel plate and are subsequently eroded. The resulting failure surface is irregular, as illustrated in Fig. 5.

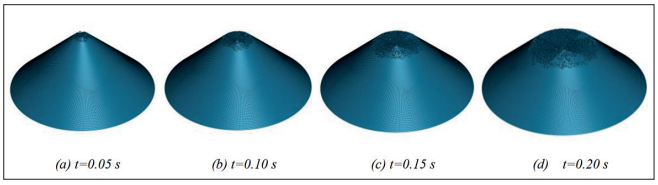

Fig. 5. Conical sea ice during the process of impact from the steel plate

The curve representing the relationship between pressure and contact area given by Palmer et al. [[26]], which serves as an important basis for describing the mechanical behaviour of ice–structure interactions, has been included in the ISO/CD 19906 (2010) standard. This curve is of great importance for the selection of sea ice parameters in polar ship design and structural engineering for ice regions. To verify the rationality of the ice material model used here, the numerical simulation results for the collision between the steel plate and the conical sea ice were compared with the theoretical curve provided in the ISO standard. The corresponding theoretical expression is as follows:

$$P = 7.4A^{-0.7} \tag{9}$$

where P denotes the contact pressure, in units of MPa, and A denotes the contact area, in units of m^2.

A comparison between the pressure–contact area curve obtained from the numerical simulation of the collision between the steel plate and the conical sea ice and the theoretical curve specified in the ISO standard [26] is shown in Fig. 6. The ISO theoretical curve follows an inverse proportional relationship, and the numerical simulation results exhibit a similar trend. In the initial stage, the contact pressure is relatively high, and it then decreases rapidly with an increase in the contact area and gradually approaches a stable level. Overall, good agreement is observed between the numerical simulation results and the ISO theoretical curve; this indicates that the mechanical properties of the sea ice material selected here satisfy the standard requirements, and confirms that the ice constitutive model is suitable for subsequent numerical simulations of ship–ice interactions.

The ice model used in this study is formulated as an isotropic elastic–plastic material with a strain-based failure criterion. The formulation has been validated against the ISO indentation pressure–area relationship, and is intended to capture the dominant crushing and fracture behaviour under the loading conditions under investigation. Rate- and temperature-dependent effects are not explicitly considered in this model, and the physical fidelity of the simulations may be further improved in future studies by incorporating these.

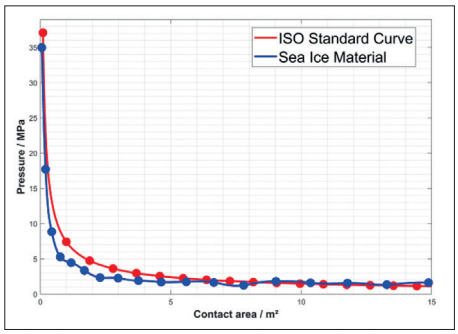

Fig. 6. Comparison between numerical simulation results and the ISO curve

NUMERICAL IMPLEMENTATION

Simulations were performed using the explicit time integration scheme in LS-DYNA. The time increment was automatically determined based on the Courant stability criterion, to ensure numerical stability. The ship–ice interaction was modelled using *CONTACT_ERODING_SURFACE_TO_SURFACE, whereas the ice–ice interaction during fragmentation was defined using *CONTACT_ERODING_SINGLE_SURFACE. A penalty-based formulation (SOFT=2) was adopted for contact enforcement. Table 5 gives the main numerical parameters of the coupled model.

Tab. 5. Summary of key numerical parameters

Structural mesh	Size of ship element	1.0 m
	Size of ice element	0.8 m
ALE mesh	Size of water element	2.0 m
	Size of air element	2.0 m
Time integration	Time step control	Courant stability criterion
Ship–ice contact	Contact type	*CONTACT_ERODING_ SURFACE_ TO SURFACE
	Friction coefficient (static)	0.1
Ice–ice contact	Contact type	*CONTACT_ERODING_ SINGLE_ SURFACE
	Friction coefficient	0.25
Ice failure model	Failure criterion	Plastic strain-based erosion
	Failure strain	0.35
Boundary conditions	Ship motion	*BOUNDARY_PRESET_ MOTION RIGID
	Fluid outer boundary	Non-reflecting boundary
Computational domain	Longitudinal extent	4 ship lengths
	Transverse extent	2 ship breadths
	Water depth	3 ship drafts

A limited mesh sensitivity check was performed for a representative case (h = 1.04 m, v = 0.2 m/s, w/B = 0.25). Following this, the size of the ice element was refined from 0.8 m to 0.7 m, while the other parameters were kept unchanged. The resulting variation in the average ice resistance was within 5%, indicating that the mesh resolution adopted in the simulations provides sufficient accuracy for the present study.

VALIDATION OF THE NUMERICAL MODEL FOR BREAKING OF LEVEL ICE

ICE TANK AND EXPERIMENTAL CONDITIONS

To validate the numerical simulation method, the test data reported by Zhou et al. [[24]] for an ice load model were adopted as the reference benchmark. Experiments were conducted in the ice tank at Aalto University using a scale model of the icebreaking tanker *MT Uikku*, with a scale ratio of 1:31.6. The experimental setup is shown in Fig. 7. The model was connected to the towing carriage via a rigid frame, and was equipped with measurement devices including a six-component force sensor and cameras. A total of six test cases were considered by varying the ice thickness and the towing speed, and in each case, the time histories of the ice loads and the ice failure patterns were recorded, with the model test data uniformly converted to full-scale values. The corresponding test conditions are given in Table 6. It should be noted that the experiments conducted by Zhou et al. [24] were limited to level ice conditions and did not consider narrow channel scenarios.

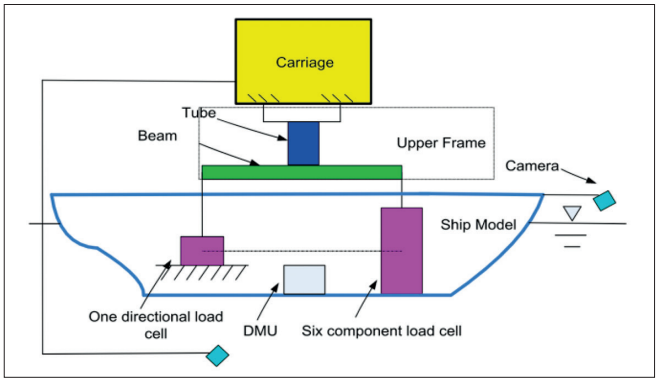

Fig. 7. Components of the experimental test system [[24]]

Note: Terminology in the figure follows the original reference [24]; the standardized nomenclature used in the text is: One-directional load cell, Upper frame, Ship model, Six-component load cell.

VALIDATION THROUGH COMPARISON OF RESULTS

Validation of ice failure patterns

Fig. 8 illustrates the breaking process of level ice during the forward motion of the ship, as simulated by the LS-DYNA numerical model under experimental condition 302. As shown in Fig. 8(a), in the initial stage of icebreaking, the bow of the ship comes into contact with the ice sheet, and local ice failure first occurs in the contact region under the compressive action of the bow, leading to the formation of fragmented ice particles. At the same time, radial and circumferential cracks gradually develop in the ice sheet, in front of and on both sides of the bow. It can be seen from Fig. 8(b) that as the ship continues to advance, block-shaped ice fragments formed from the intersection of radial and circumferential cracks detach from the ice sheet and are pushed aside, along both sides of the hull, by the bow. As shown in Fig. 8(c), the intact ice sheet ahead comes into contact with the bow again and is subjected to compression; new cracks are continuously generated in the ice sheet, meaning that the icebreaking process has a continuous nature. The bottom view in Fig. 8(d) shows that under the combined effects of the ship's motion and the surrounding water, the generated ice fragments adhere to the surface of the hull and slide backward along it. After the bow has entered the ice sheet, broken ice is distributed within the ice channel. As the ship continues to move forward, the broken ice is transported by the hull and gradually accumulates along both sides of the ice channel.

Tab. 6. Experimental test conditions

Test ID	Ice thickness (m)	Ship speed (m/s)
301	1.04	0.2
302	1.04	0.5
303	1.04	1.0
401	0.63	0.2
402	0.63	0.5
403	0.63	1.0

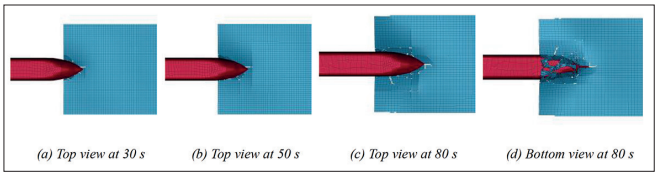

Fig. 8. Numerical simulation results for the failure process of level ice during forward motion of the ship

To verify the rationality of the LS-DYNA numerical model, the local ice failure patterns observed in the ice tank experiments were compared with those obtained from the LS-DYNA numerical simulations of the interaction between the ship hull and level ice. Fig. 9(a) shows the failure observed in the ice tank experiments under level ice conditions, and it can be seen that pronounced ice cracking occurs in the contact region between the hull and the ice sheet, with circumferential cracks and block-shaped ice fragments forming on one side of the hull. Fig. 9(b) presents the numerical simulation results obtained under the same test conditions, in which local ice failure is also observed in the vicinity of the hull, showing good agreement with the experimental observations. This comparison demonstrates that the numerical simulation reasonably reproduces the failure patterns of level ice observed in the experiments, indicating that the established ship–ice interaction numerical model has satisfactory reliability in terms of describing the local failure characteristics of level ice.

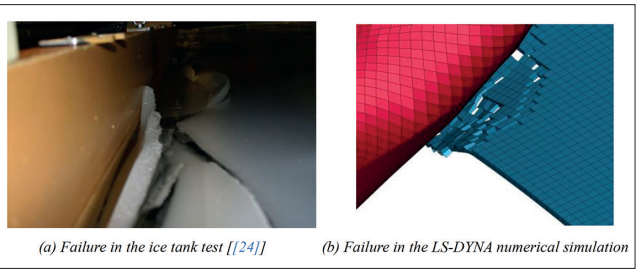

(a) Failure in the ice tank test [[24]] (b) Failure in the LS-DYNA numerical simulation

Fig. 9. Comparison of modes of failure for level ice in the ice tank test and numerical simulation

Comparison of resistance

Fig. 10 presents time histories of the ship resistance in level ice under the different test conditions listed in Table 6, with the corresponding mean resistance values. It can be observed that the resistance obtained from the numerical simulations exhibits pronounced temporal fluctuations, which are mainly related to the repeated processes of compression, fracture, and subsequent resistance release of the ice sheet under the action of the ship's bow. A statistical analysis of the resistance time histories shows that the mean resistance values are relatively close to those obtained from the ice tank experiments. Fig. 11 shows the relative errors between the numerically predicted and experimentally measured mean resistance values for each test condition, with errors mainly distributed within the range 8–11%. These results indicate that the numerical model established in this study is capable of reasonably predicting the resistance level of a ship under continuous icebreaking conditions in level ice.

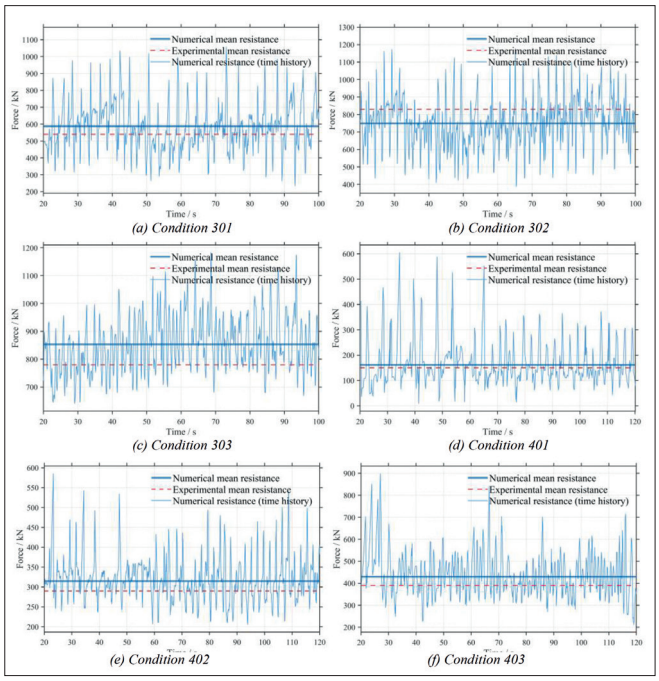

Fig. 10. Time histories and mean values of ship resistance in level ice under different conditions

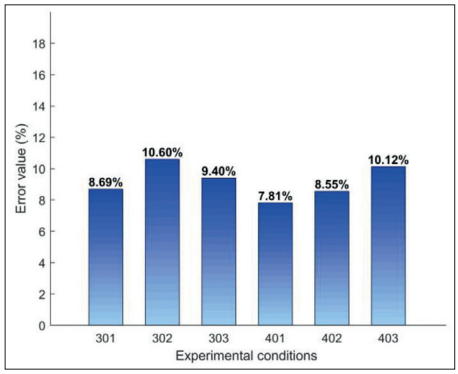

Fig. 11. Relative errors between numerical and experimental values for the mean ice resistance

NUMERICAL SIMULATION OF SHIP ICEBREAKING RESISTANCE IN NARROW CHANNELS IN ICE-COVERED AREAS

After the numerical model had been validated under level ice conditions, a corresponding narrow ice channel model was established to enable further investigation of the ship's icebreaking resistance in confined channels. Compared with level ice conditions, the contact characteristics between the ship hull and ice change during navigation in narrow channels, leading to distinct differences in the icebreaking resistance. This section focuses on the magnitude of the ship's icebreaking resistance under narrow ice channel conditions. We varied the channel width, ship speed, and ice thickness to compare the icebreaking resistance under different conditions, and systematically analysed the influence of each parameter. Based on the validated numerical model, a series of simulations were conducted involving narrow ice channels. Ship speeds of 0.2, 0.5, and 1.0 m/s were selected to represent low-, medium-, and high-speed icebreaking conditions. Two ice thicknesses of 1.04 and 0.63 m were considered to examine the effect of ice thickness. Based on the definition of narrow ice channels given above, three non-dimensional channel widths, $\gamma = 0.25$, 0.5, and 0.75, were adopted to represent different degrees of channel confinement. The details of each simulation condition are given in Table 7.

Tab. 7. Settings for the numerical simulations under 18 conditions

Test ID	501	502	503	601	602	603	701	702	703
v/(m/s)	0.20	0.50	1.0	0.20	0.50	1.0	0.20	0.50	1.0
h/m	1.04	1.04	1.04	1.04	1.04	1.04	1.04	1.04	1.04
γ	0.25	0.25	0.25	0.5	0.5	0.5	0.75	0.75	0.75
Test ID	801	802	803	901	902	903	1001	1002	1003
v/(m/s)	0.20	0.50	1.0	0.20	0.50	1.0	0.20	0.50	1.0
h/m	0.63	0.63	0.63	0.63	0.63	0.63	0.63	0.63	0.63
γ	0.25	0.25	0.25	0.5	0.5	0.5	0.75	0.75	0.75

To enable clearer physical interpretation of the geometric configurations, the corresponding full-scale channel widths for each non-dimensional value γ are given in Table 8.

Tab. 8. Physical channel widths corresponding to different non-dimensional channel widths

γ	Channel width w
0	0
0.25	5.25
0.50	10.50
0.75	15.75
1	21

PHYSICAL PROCESS OF NARROW ICE CHANNEL EFFECTS

In a narrow ice channel, the width of the channel is one of the primary factors influencing the icebreaking process. Numerical simulations were conducted for channels of different widths to investigate the evolution of ice fracture patterns at different icebreaking stages, and to analyse the influence of channel confinement. To ensure consistency in the icebreaking process and reduce the computational cost, the initial positions of all ships were uniformly set so that contact with the ice layer occurred within 1 s.

Fig. 12 illustrates the temporal evolution of the ice fracture patterns as the ship advanced in a narrow ice channel under different channel width conditions. As shown in Fig. 12(a), in the initial stage (t = 15 s), the ship bow has just contacted the ice layer, and the ice remains largely intact for all channel widths. Ice fracture is mainly limited to local crushing in front of the bow, accompanied by a few radial cracks, and the differences among the channel widths are not significant. It can be seen from Fig. 12(b) that at t = 30 s, distinct differences in ice fracture patterns have begun to emerge. In wider channels, ice fracture remains concentrated near the bow and propagates primarily along the direction of sailing, with a relatively limited affected area. In contrast, in narrower channels, ice fracture extends laterally toward the channel boundaries due to spatial confinement, and shear-dominated failure becomes evident. Fig. 12(c) shows a later stage of icebreaking (t = 80 s), in which these differences are further amplified. In wider channels, the area of ice fracture remains stable and confined near the bow, whereas in narrower channels, increased contact between the ice layer, ship bow and channel boundaries leads to a more extensive area of fracture, with shear-dominated damage becoming more pronounced. The observed differences in the ice fracture patterns reflect the influence of spatial confinement on ship–ice interaction, and provide a physical basis for the subsequent analysis of fluctuations in icebreaking resistance.

Fig. 13(a) and (b) illustrate the stress distribution of the ice layer at different times for the case with a non-dimensional channel width of 0.25, as an example. It can be observed that under narrow channel conditions, the stress distribution in the ice is characterised by pronounced nonuniformity, with high-stress regions mainly concentrated near the bow of the ship and along the channel boundaries. At earlier times, the high-stress regions are primarily distributed in front of and around the bow, forming

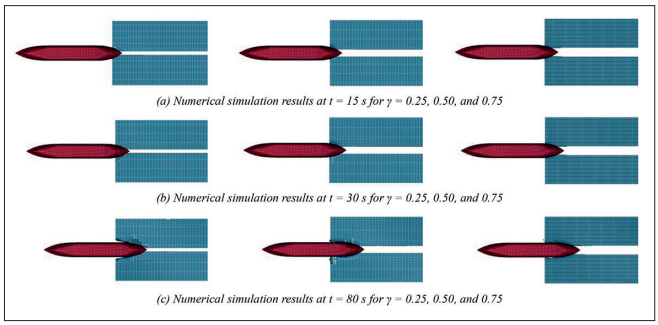

Fig. 12. Numerical simulation results for different channel widths

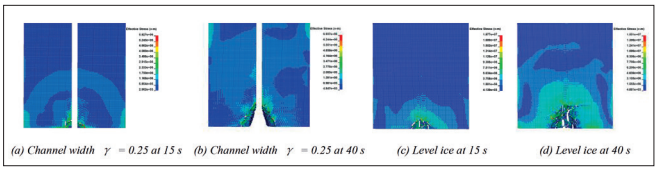

Fig. 13. Ice stress distributions at different times (units: Pa)

a ring-shaped stress band along the outer edge of the bow. As time progresses, the high-stress regions gradually extend toward the channel boundaries and become increasingly dispersed, eventually forming relatively continuous stress concentration zones near the channel boundaries. A comparison of Fig. 13(c) and (d) under level ice conditions shows that the distribution patterns of high-stress regions in the ice layer are generally similar under the two conditions, indicating that the narrow channel condition does not significantly alter the local stress characteristics of the ice layer induced by the ship bow, although the ice resistance under level ice conditions is significantly greater than that under narrow channel conditions.

RESULTS FOR ICEBREAKING RESISTANCE IN NARROW CHANNELS

Time histories of icebreaking resistance for a ship navigating in a narrow ice channel under different working conditions are presented in Fig. 14. Each subfigure shows the variation in the resistance with time for different non-dimensional channel widths (γ = 0.25, 0.50, and 0.75) for a specific combination of ship speed and ice thickness.

The icebreaking resistance exhibits pronounced temporal fluctuations, and the characteristics of these fluctuations are strongly influenced by the channel width, ship speed, and ice thickness. In narrower channels (γ = 0.25), both the fluctuation amplitude and the instantaneous peak values of resistance are relatively large, whereas with increasing channel width (γ = 0.50 and 0.75), the variation in the resistance becomes smoother and the fluctuation amplitude decreases. As shown in Fig. 14(a) and (d), under low ship speed conditions (0.2 m/s), the fluctuations are relatively mild and the time histories remain stable; with an increase in speed, as illustrated in Fig. 14(c) and (f), the fluctuation amplitude and peak resistance increase significantly, particularly under narrow channel conditions. Comparisons among Fig. 14(a)–(c) and (d)–(f) indicate that a larger ice thickness (1.04 m) leads to higher resistance levels and stronger fluctuations, whereas thinner ice (0.63 m) results in reduced fluctuation intensity and lower peak values.

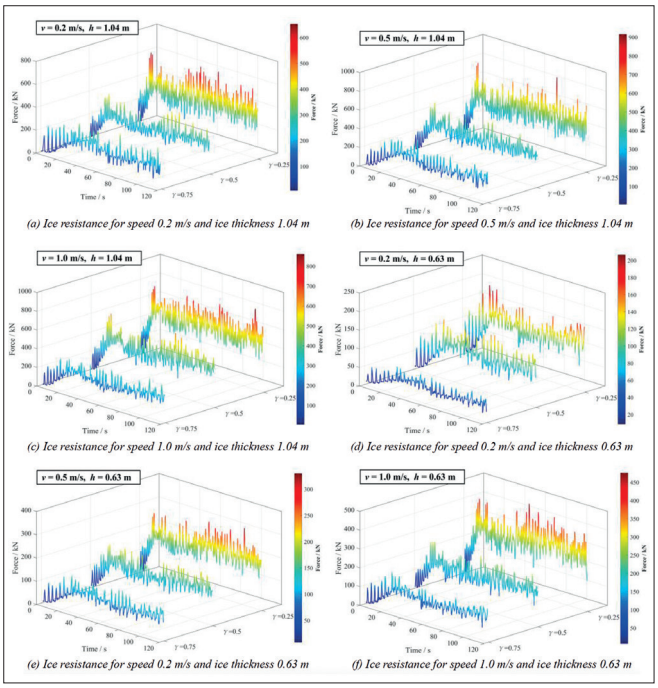

(a) Ice resistance for speed 0.2 m/s and ice thickness 1.04 m
(b) Ice resistance for speed 0.5 m/s and ice thickness 1.04 m
(c) Ice resistance for speed 1.0 m/s and ice thickness 1.04 m
(d) Ice resistance for speed 0.2 m/s and ice thickness 0.63 m
(e) Ice resistance for speed 0.2 m/s and ice thickness 0.63 m
(f) Ice resistance for speed 1.0 m/s and ice thickness 0.63 m

Fig. 14. Time histories of ship icebreaking resistance in narrow ice channels under different conditions

DISCUSSION

The icebreaking resistance of a ship can be interpreted as the combined result of ice failure and fragment clearing processes [27]. Ice failure involves flexural bending and local crushing, while fragment clearing includes the displacement and buoyancy-driven motion of broken ice along the hull. In the following discussion, the influence of channel geometry, ship speed and ice thickness is analysed in terms of the evolving balance among these mechanisms and their associated energy dissipation characteristics.

EFFECT OF CHANNEL WIDTH ON ICE RESISTANCE

To evaluate the dependence of icebreaking resistance on channel width, the average resistance under different non-dimensional channel widths γ was analysed as shown in Fig. 15. Additional numerical cases with $\gamma = 0.1$ were introduced for each working condition to enable the structural response to be captured better for extremely narrow channels. A quadratic polynomial was adopted to describe the resistance variation within confined channel configurations; however, this fitting is intended to represent only the mechanical response under geometric confinement, and does not imply structural equivalence with intact level ice at $\gamma = 0$. From a physical standpoint, channel confinement alters the load-transfer mechanism between the ship and the ice sheet. Unlike intact level ice, the confined configuration already has lateral free boundaries and a partially fractured region, meaning that the failure mode and the associated resistance components are fundamentally modified.

As shown in Fig. 15(a)–(f), the average resistance decreases with increasing γ, and the reduction exhibits clear stage-dependent characteristics. In the small-γ region, resistance is highly sensitive to channel width, since the effective bending span of the ice sheet changes rapidly with slight geometric separation: even a small lateral clearance significantly reduces the flexural continuity of the plate, thereby decreasing the bending component of resistance. As γ increases further, the bending span becomes relatively stabilised, and the reduction rate gradually decreases, indicating that the contribution of flexural resistance has already been substantially weakened. The region marked in red in Fig. 15 highlights the deviation between the experimentally measured resistance under level ice conditions and the extrapolated resistance at $\gamma = 0$. The persistence of this deviation confirms that the global plate behaviour of intact level ice cannot be reconstructed for an almost closed channel configuration. Even when γ approaches zero, the presence of lateral boundaries prevents the re-establishment of large-scale bending deformation, and the flexural energy consumption therefore remains lower than for true level ice.

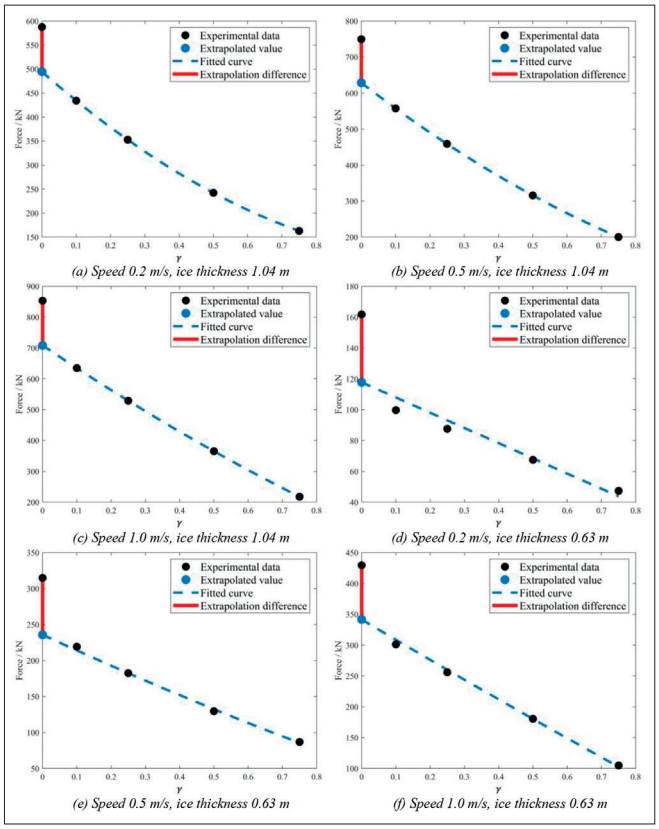

(a) Speed 0.2 m/s, ice thickness 1.04 m
(b) Speed 0.5 m/s, ice thickness 1.04 m
(c) Speed 1.0 m/s, ice thickness 1.04 m
(d) Speed 0.2 m/s, ice thickness 0.63 m
(e) Speed 0.5 m/s, ice thickness 0.63 m
(f) Speed 1.0 m/s, ice thickness 0.63 m

Fig. 15. Average ice resistance and fitted curves under different channel widths

Fig. 16 further quantifies this deviation by showing the difference between the level ice resistance and the extrapolated resistance at $\gamma = 0$. The positive values observed for all calculated cases confirm that the confined configuration consistently produces a lower resistance than intact level ice. For a given ice thickness, the magnitude of this deviation increases with ship speed, suggesting that at higher speeds, the energy demand associated with global bending deformation in level ice becomes more pronounced, whereas the confined configuration suppresses large-scale deformation. Consequently, the relative reduction in flexural energy consumption becomes more evident as the speed increases. The increasing deviation with speed reflects not merely

a numerical difference but a transition in the dominant energy dissipation mechanisms between continuous plate bending and localised crushing–fragmentation processes.

To facilitate a comparison among the different conditions, the difference in resistance was normalised based on the corresponding level ice resistance, and the results are shown in Fig. 17. The relative trends remain consistent across all cases: as γ increases, the reduction ratio increases, although the growth rate decreases markedly for $\gamma \geq 0.25$. In mechanistic terms, this behaviour reflects the progressive reduction of the flexural component of resistance as geometric confinement intensifies. In extremely narrow channels, the icebreaking process shifts from global penetration and large-scale bending of a continuous plate to predominantly localised crushing, secondary fragmentation, and fragment clearing along the hull. From an energy perspective, channel confinement weakens bending-related energy consumption, resulting in a lower total resistance even when γ approaches zero. This explains why the extrapolated value at $\gamma = 0$ does not coincide with the directly simulated level ice resistance: the structural and energy dissipation mechanisms remain fundamentally different.

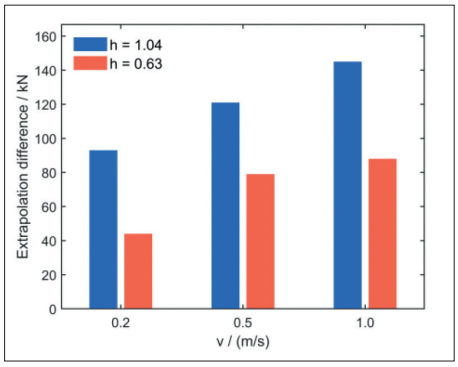

Fig. 16. Differences between the experimental values under level ice conditions and extrapolated values from the fitted curve

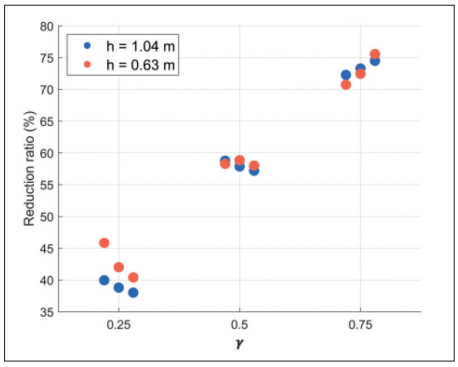

Fig. 17. Percentage difference in resistance between narrow ice channel and level ice, normalized by level ice resistance

EFFECT OF SHIP SPEED ON ICE RESISTANCE

To evaluate the influence of the ship's speed on the icebreaking resistance in narrow channels, the variation in the average resistance with ship speed is presented in Fig. 18. For all values of the channel width and ice thickness, the resistance increases monotonically with ship speed. For example, at $\gamma = 0.25$, the average resistance rises from approximately 353 kN at 0.2 m/s to about 529 kN at 1.0 m/s, corresponding to an increase of nearly 50%. The difference in resistance between the level ice condition ($\gamma = 0$) and the narrow channel condition ($\gamma = 0.75$) also becomes more pronounced at higher speeds, suggesting that ship speed amplifies the influence of geometric confinement.

A closer examination shows that the rate of growth in the resistance gradually decreases in the higher range of speeds. For $\gamma = 0.25$, the increase from 0.2 m/s to 0.5 m/s is approximately 106 kN, whereas the increment from 0.5 m/s to 1.0 m/s is about 70 kN. As stated in Section 2, the ice model adopted here represents a simplified elastic–plastic constitutive formulation, without explicit dependence on strain rate or temperature. The observed speed dependence should therefore be interpreted within the framework of these modelling assumptions.

Within this context, a higher ship speed is associated with more intensive local crushing, accelerated fragment motion and increased energy dissipation through fracture and fragment clearing. In narrow channels, lateral confinement restricts fragment dispersion and promotes repeated contact along the channel edges, thereby enhancing the relative contribution of crushing and clearing mechanisms while reducing the dominance of large-scale bending deformation. Consequently, the speed effect can be interpreted as a gradual shift from bending-dominated behaviour towards dynamically driven crushing and fragmentation under confined conditions.

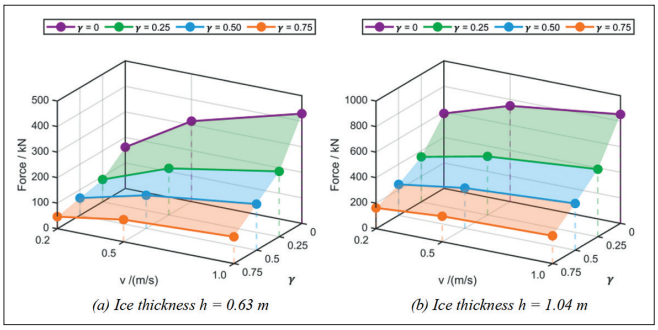

Fig. 18. Average ice resistance at different ship speeds in narrow channels in ice-covered waters, for two different values of ice thickness

EFFECT OF ICE THICKNESS ON ICE RESISTANCE

The variation in the average icebreaking resistance with ship speed for two different ice thicknesses and several channel-width conditions is shown in Fig. 19. Taking $\gamma = 0.25$ as an example, it can be seen from Fig. 19(b) that when the ship's speed is 0.2 m/s, the resistances for $h = 1.04$ m and $h = 0.63$ m are 352.73 kN and 87.58 kN, respectively, resulting in a difference of 265.15 kN. When the channel width is increased to $\gamma = 0.75$, as shown in Fig. 19(d), at a ship speed of 0.2 m/s, the resistances for $h = 1.04$ m and $h = 0.63$ m are 162.84 kN and 47.31 kN, respectively, with a difference of 115.53 kN. At a ship speed of 1.0 m/s, the resistances for $h = 1.04$ m and $h = 0.63$ m are 217.55 kN and 104.94 kN, respectively, with a difference of 112.61 kN. This indicates that wider channel conditions moderate the influence of ice thickness.

In mechanistic terms, the thickness of the ice primarily affects the flexural stiffness and fracture resistance of the ice sheet: thinner ice tends to fail rapidly through bending, with limited energy consumption, whereas thicker ice requires greater bending work and maintains higher resistance over a longer advancing distance. This enhances the flexural component of the total resistance and increases the average load level. As the channel width increases, lateral confinement weakens and the effective bending span is reduced, limiting large-scale flexural deformation. Consequently, the relative contribution of bending decreases, and the difference in the resistance of thick and thin ice becomes less pronounced. Nevertheless, the ice thickness still governs the overall resistance level, since crushing and fragment clearing also scale with the thickness.

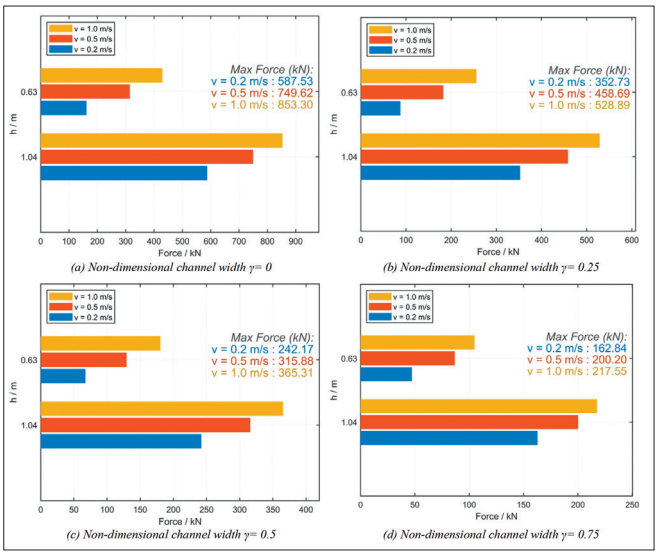

Fig. 19. Average ice resistance under different ice thicknesses in narrow channels in ice-covered waters

SCOPE AND APPLICABILITY OF THE MODEL

The numerical framework adopted in this study was developed to investigate the influence of geometric confinement on global icebreaking resistance in narrow channels. To ensure computational tractability while isolating the mechanical effect of channel width, several modelling idealisations were introduced. The ship was treated as a rigid body, since the primary objective was to evaluate the overall resistance rather than the structural response. In addition, within the range of values investigated for the ice thickness and speed, the average resistance was predominantly governed by ice fracture and contact processes, and the elastic deformation of the hull was not expected to have a significant influence on the global resistance level. The channel simulated here involved an idealised icebreaker-cleared condition in which intact ice along the channel boundaries represented the dominant component of resistance. Residual broken ice within the channel was not explicitly modelled, to allow the confinement effect associated with the channel width to be examined in a controlled manner.

The channel boundaries were also assumed to be straight and geometrically uniform, to enable a consistent comparison among different non-dimensional channel widths γ, and modelling of the natural irregularities and stochastic features of ice fell outside the scope of the present work. Within these assumptions, the model provides a physically consistent framework for analysing mechanisms governing the variation in resistance under confined conditions, and is primarily applicable to relatively clean escort channels within the range of ship speeds and ice thicknesses investigated here.

CONCLUSION

This study has focused on the problem of the icebreaking resistance of a ship under narrow-channel conditions in ice-covered waters. A numerical model of the ship–ice–water interaction was established using an explicit dynamics approach, and the icebreaking process and ice resistance characteristics under varying values for the channel width, ship speed, and ice thickness were systematically investigated. The main findings can be summarised as follows:

(1) A numerical case involving a steel plate impacting on conical sea ice was investigated, and the simulated relationship between contact pressure and contact area was compared with the theoretical curve specified in ISO 19906. The results indicated that good agreement was achieved in terms of both the variation trend and the order of magnitude, thus verifying the effectiveness of the sea ice constitutive model adopted for numerical simulations of ship icebreaking.

(2) A coupled numerical model of the ship–ice–water interaction was established and validated through comparison with the results of ice tank model tests, in terms of ice failure patterns and average icebreaking resistance. The numerical results showed good agreement with the experimental results, indicating that the model was reliable in predicting icebreaking resistance and describing the failure behaviour of ice.

(3) The channel width was found to have a significant influence on the icebreaking resistance of the ship. The results showed that the average resistance decreased monotonically with an increase in the non-dimensional channel width γ, and the reduction was more pronounced when γ was small. When the value of γ exceeded approximately 0.25, the rate of reduction became more moderate. A comparison with the breaking of intact level ice indicated that the confined channel configurations had a structurally different resistance mechanism, meaning that the extrapolated value for $\gamma = 0$ does not coincide with the directly simulated resistance for level ice.

(4) The speed of the ship and the thickness of the ice were found to have a significant effect on icebreaking resistance in narrow channels. The average icebreaking resistance increased with both the ship speed and ice thickness. Under conditions with relatively narrow channels, the amplification effect of the ship speed and ice thickness on resistance was more pronounced than under level ice conditions.

The characteristics of the variation in ship icebreaking resistance under narrow-channel conditions were analysed based on numerical simulations, but further validation will be required under more complex channel geometries and realistic boundary conditions. In future work, the incorporation of more advanced constitutive formulations and dedicated material parameter sensitivity analyses may be considered in order to further enhance the robustness and generality of the simulations. Future studies may also involve different types of ship and bow forms to extend the applicability of the present analysis to a wider range of operational scenarios.

FUNDING AGENCY

Supported by the Joint Program Project of Liaoning Provincial Science and Technology Program under Grant No. 2025-MSLH-079, the Fundamental Research Funds for the Central Universities" with grant No. 3132025144, the Fundamental Research Funds for the Central Universities" with grant No. 3132025143, the "University Fundamental Research Project of the Education Department of Liaoning Province" with grant No. LJ212510151010, Zhejiang Provincial Natural Science Foundation of China under Grant No. LQN26E090008, and Ningbo Natural Science Foundation under Grant No. 2025J047.

REFERENCES

1. Zhao Q, Ma J, Li Z, Guo W. Experimental study of ship oblique motion in floating ice of different concentrations. J. Mar. Sci. Eng. 2025, vol. 13, p. 2403. https://doi.org/10.3390/jmse13122403

2. Li F, Lu L, Puolakka O, Kujala P. Ice channel breakout performance of a double-acting vessel. Ocean Eng 2024, vol. 293, p. 116657. https://doi.org/10.1016/j.oceaneng.2023.116657

3. Han D, Qiao Y, Xue Y, Wang X. A review of research methods for ice resistance of ships navigating in ice-covered waters. J. Ship Mech. 2017, vol. 21, pp. 1041–1054.

4. Riska K, Leiviskä T, Nyman T, Fransson L, Lehtonen J, Eronen H, Backman A. Ice performance of the Swedish multi-purpose icebreaker Tor Viking II. Proc. Int. Conf. Port Ocean Eng. under Arctic Conditions (POAC), Ottawa, Canada, 2001.

5. Zhou L, Riska K, Polach RVB, Kujala P. Experiments on level ice loading on an icebreaking tanker with different ice drift angles. Cold Reg. Sci. Technol. 2013, vol. 85, pp. 79–93. https://doi.org/10.1016/j.coldregions.2012.09.007

6. Lindqvist G. A straightforward method for calculation of ice resistance of ships. Proc. Int. Conf. Port Ocean Eng. under Arctic Conditions (POAC), Luleå, Sweden, 1989.

7. Keinonen AJ, Browne RP. Icebreaker performance prediction. Trans. Soc. Nav. Archit. Mar. Eng. 1991, vol. 99, pp. 221–248.

8. Riska K, Englund K. Research Report No 52 Performance of merchant vessels in ice in the Baltic. Helsinki University of Technology, Helsinki, Finland, 1997.

9. Spencer D, Jones SJ. Model-scale/full-scale correlation in open water and ice for Canadian Coast Guard "R-class" icebreakers. J. Ship Res. 2001, vol. 45, pp. 249–261.

10. Zou M, Tang XJ, Zou L, Wang H, Li Y. Numerical investigations of the restriction effects on a ship navigating in pack-ice channel. Ocean Eng. 2024, vol. 305, p. 117968. https://doi.org/10.1016/j.oceaneng.2024.117968

11. Ren Y, Chen Z, He Y, Zhang Z, Wang J. Numerical analysis of continuous icebreaking performance of icebreakers with different bow types. Ocean Eng. 2023, vol. 269, p. 113712. https://doi.org/10.1016/j.oceaneng.2022.113712

12. Bian A, Chai W, Dong H, Yu Z, Leira BJ, Xiong F. Strength analysis of icebreaker ramming sea ice with extreme thickness along the Northern Sea Route. Proc. ASME Int. Conf. Ocean Offshore Arctic Eng. (OMAE), 2024.

13. Diao ZT, Fang DJ, Cao JW. Numerical study on interaction between the water-exiting vehicle and ice based on FEM-SPH-SALE coupling algorithm. Appl. Sci. 2025, vol. 15, p. 8318. https://doi.org/10.3390/app15158318

14. Xu P, Chen B, Guo Y, Wang H. Numerical simulation study on ice-water-ship interaction based on FEM-SPH adaptive coupling algorithm. Water 2024, vol. 16, p. 3249. https://doi.org/10.3390/w16223249

15. Liu D, Zhang S, Liu Z, Gu Z, Zhang L, Liu Z. Numerical simulation study of ship–ice interaction based on multi-fracture strength cohesive element model. Ships Offshore Struct. 2026-03-22. Retrieved from https://doi.org/10.1080/17445302.2025.2452081

16. Gagnon RE. A numerical model of ice crushing using a foam analogue. Cold Reg. Sci. Technol. 2011, vol. 65, pp. 335–350. https://doi.org/10.1016/j.coldregions.2010.11.007

17. Kim J, Yoon DH, Choung J. Numerical study of ship hydrodynamics on ice resistance during ice sheet breaking. Ocean Eng. 2024, vol. 308, p. 118285. https://doi.org/10.1016/j.oceaneng.2024.118285

18. Xu Y, Hu Z, Ringsberg JW, Li Z. An ice material model for assessment of strain rate, temperature and confining pressure effects using finite element method. Ships Offshore Struct. 2019, vol. 14, pp. S34–S44. https://doi.org/10.1080/17445302.2018.1559197

19. Sazonov K, Dobrodeev A. Ice resistance assessment for a large size vessel running in a narrow ice channel behind an icebreaker. J. Mar. Sci. Appl. 2021, vol. 20, pp. 446–455. https://doi.org/10.1007/s11804-021-00212-3

20. Fang L, Suominen M, Kuuja P. Ship performance in ice channels narrower than ship beam: Model test and numerical investigation. Ocean Eng. 2021, vol. 240, p. 109922. https://doi.org/10.1016/j.oceaneng.2021.109922

21. Dong HB, Xia JS, Liu JJ, Gao YJ, Wang ZL. Study on structural response characteristics of ships in ice-covered narrow channels. Ship Sci. Technol. 2025, vol. 47, pp. 54–60.

22. Huang L, Li M, Romu T, Dolatshah A, Thomas G. Simulation of a ship operating in an open-water ice channel. Ships Offshore Struct. 2021, vol. 16, pp. 353–362. https://doi.org/10.1080/17445302.2020.1760304

23. Bathe KJ. Finite element procedures. 2nd ed. Cambridge: Klaus-Jürgen Bathe; 2014.

24. Zhou L, Chuang ZJ, Ji CY. Ice forces acting on towed ship in level ice with straight drift. Part I: Analysis of model test data. Pol. Marit. Res. 2018, vol. 25, pp. 60–68. https://doi.org/10.2478/pomr-2018-0008

25. Shi YH, Yang DQ, Wu WW. Numerical analysis method of ship–ice collision-induced vibration of the polar transport vessel based on the full coupling of ship–ice–water–air. J. Ocean Eng. Sci. 2023, vol. 8, pp. 323–335. https://doi.org/10.1016/j.joes.2022.08.006

26. Palmer AC, Dempsey JP, Masterson DM. A revised ice pressure–area curve and a fracture mechanics explanation. Cold Reg. Sci. Technol. 2009, vol. 56, pp. 73–76. https://doi.org/10.1016/j.cldregions.2008.10.007

27. International Towing Tank Conference (ITTC), "Resistance tests in ice," ITTC Recommended Procedures and Guidelines, 7.5-02-04-02.1, 2017. [Online]. Available: https://www.ittc.info/media/8053/75-02-04-021